SMC-TR-05-11

AEROSPACE REPORT NO.
TR-2005(8555)-1

Porosity Characteristics of Nickel Sinter

15 February 2005

Prepared by

A. H. ZIMMERMAN and G. A. TO
Electronics and Photonics Laboratory
Laboratory Operations

Prepared for

SPACE AND MISSILE SYSTEMS CENTER
AIR FORCE SPACE COMMAND
2430 E. El Segundo Boulevard
Los Angeles Air Force Base, CA 90245

Engineering and Technology Group

THE AEROSPACE CORPORATION
El Segundo, California

This report was submitted by The Aerospace Corporation, El Segundo, CA 90245-4691, under Contract No. FA8802-04-C-0001 with the Space and Missile Systems Center, 2430 E. El Segundo Blvd., Los Angeles Air Force Base, CA 90245. It was reviewed and approved for The Aerospace Corporation by B. Jaduszliwer, Principal Director, Electronics and Photonics Laboratory. Michael Zambrana was the project officer for the Mission-Oriented Investigation and Experimentation (MOIE) program.

This report has been reviewed by the Public Affairs Office (PAS) and is releasable to the National Technical Information Service (NTIS). At NTIS, it will be available to the general public, including foreign nationals.

This technical report has been reviewed and is approved for publication. Publication of this report does not constitute Air Force approval of the report's findings or conclusions. It is published only for the exchange and stimulation of ideas.

Michael Zambrana
SMC/AXE

REPORT DOCUMENTATION PAGE

Form Approved
OMB No. 0704-0188

1. REPORT DATE (*DD-MM-YYYY*)	2. REPORT TYPE	3. DATES COVERED *(From - To)*
15-02-2005		

4. TITLE AND SUBTITLE

Porosity Characteristics of Nickel Sinter

5a. CONTRACT NUMBER
FA8802-04-C-0001

5b. GRANT NUMBER

5c. PROGRAM ELEMENT NUMBER

6. AUTHOR(S)

A. H. Zimmerman and G. A. To

5d. PROJECT NUMBER

5e. TASK NUMBER

5f. WORK UNIT NUMBER

7. PERFORMING ORGANIZATION NAME(S) AND ADDRESS(ES)

The Aerospace Corporation
Laboratory Operations
El Segundo, CA 90245-4691

8. PERFORMING ORGANIZATION REPORT NUMBER

TR-2005(8555)-1

9. SPONSORING / MONITORING AGENCY NAME(S) AND ADDRESS(ES)

Space and Missile Systems Center
Air Force Space Command
2450 E. El Segundo Blvd.
Los Angeles Air Force Base, CA 90245

10. SPONSOR/MONITOR'S ACRONYM(S)
SMC

11. SPONSOR/MONITOR'S REPORT NUMBER(S)
SMC-TR-05-11

12. DISTRIBUTION/AVAILABILITY STATEMENT

Approved for public release; distribution unlimited.

13. SUPPLEMENTARY NOTES

14. ABSTRACT

The porosity characteristics of sintered-nickel plaque made by a range of manufacturing processes for use in the nickel electrodes in nickel hydrogen cells have been measured. These characteristics include variations in porosity and pore size through the thickness of the sinter, as well as the uniformity of the sinter. Sinter made using an aqueous slurry process is found to provide the uniformity typically found in dry-powder sinter processes, with the smaller pore sizes typically associated with the alcohol-based slurry sinter process.

15. SUBJECT TERMS

Sinter, Nickel electrodes, Nickel-hydrogen cells, Batteries, Porosity, Porosimetry

16. SECURITY CLASSIFICATION OF:			17. LIMITATION OF ABSTRACT	18. NUMBER OF PAGES	19a. NAME OF RESPONSIBLE PERSON
a. REPORT	b. ABSTRACT	c. THIS PAGE			Albert Zimmerman
UNCLASSIFIED	UNCLASSIFIED	UNCLASSIFIED		27	19b. TELEPHONE NUMBER *(include area code)* (310)336-7415

Contents

1. Introduction 1
2. Sinter Samples 3
3. Porosimetry Measurement and Analysis Method 5
4. Unique Sinter Structures 9
   - 4.1 Unusual Sinter Voids 9
   - 4.2 Unusual Sinter Aggregates 12
5. Porosimetry Results 15
   - 5.1 Alcohol-Based Slurry Sinter 15
   - 5.2 Water-Based (Aqueous) Slurry Sinter 19
   - 5.3 Dry-Powder Sinter 21
6. Discussion of Results 25
7. Conclusions 27

Figures

1. Typical SEM image of a cross-sectioned sinter sample. 5
2. Distribution of the pixel luminosity over a typical 1200- by 960-μm SEM image of a cross-sectioned nickel sinter sample. 6
3. Large void frequently seen in alcohol-based slurry sinter away from the center grid-containing region 9
4. Large voids frequently seen in alcohol-based slurry sinter in proximity with the center grid wires. 10
5. Center void that has thinned down to appear more like a crack that is occasionally seen in slurry sinter. 11

6. Void commonly seen in dry-powder nickel sinter where the powder has separated from the grid wires 11

7. Horizontal crack or void occasionally seen on the side of dry-powder sinter where there are no supporting grid wires 12

8. High-density aggregates of nickel powder frequently seen in alcohol-based slurry nickel sinter. 13

9. Surface aggregate or lump of high-density nickel powder seen infrequently (once) for water-based slurry nickel sinter. 13

10. Nickel particles sintered into a closed-loop chain in a dry-powder sinter sample. 14

11. Needle-shaped nickel fragment seen in one sample of dry-powder nickel sinter. 14

12. Changes in the pore size distribution through the thickness of a typical sample of alcohol-based slurry sinter. These data are from sample 2D. 15

13. Variation in the average pore size through the thickness of alcohol-based slurry sinter samples from Group 1. 16

14. Variation in the average sinter porosity through the thickness of alcohol-based slurry sinter samples from Group 1. 17

15. Variation in the average pore size through the thickness of alcohol-based slurry sinter samples from Group 2. 17

16. Variation in the average sinter porosity through the thickness of alcohol-based slurry sinter samples from Group 2 18

17. Variation in the average pore size through the thickness of alcohol-based slurry sinter samples from Group 3. 18

18. Variation in the average sinter porosity through the thickness of alcohol-based slurry sinter samples from Group 3 19

19. Changes in the pore size distribution through the thickness of a typical sample of water-based (aqueous) slurry sinter 20

20. Variation in the average pore size through the thickness of water-based (aqueous) slurry sinter samples from Group 6 20

21. Variation in the average sinter porosity through the thickness of water-based (aqueous) slurry sinter samples from Group 6 21

22. Changes in the pore size distribution through the thickness of a typical sample of dry-powder sinter. These data are from sample 4A. 22

23. Variation in the average pore size through the thickness of dry-powder sinter samples from Group 4. 23

24. Variation in the average sinter porosity through the thickness of dry-powder sinter samples from Group 4 23

25. Variation in the average pore size through the thickness of dry-powder sinter samples from Group 5. 24

26. Variation in the average sinter porosity through the thickness of dry-powder sinter samples from Group 5 24

27. Variability in pore size (as a percentage of overall average pore size) for each type of sinter. 25

28. Variability in sinter porosity (as a percentage of overall average sinter porosity) for each type of sinter. 26

Table

1. Sinter Samples Analyzed..... 3

1. Introduction

The nickel electrodes that are used in nickel-hydrogen cells require a well-made sintered-nickel plaque as a substrate in their production. If the sintered-nickel plaque contains large voids, surface protrusions, or other kinds of defects, it will not generally allow the production of high-performance nickel electrodes. A number of processes are presently used for producing the sintered-nickel plaque used in nickel-hydrogen cells. The principal processes include:

Process 1: Alcohol-based slurry process.

Process 2: Dry-powder process.

Process 3: Water-based, or aqueous slurry process.

The slurry processes mix the nickel powder with pore-forming materials into either a water- or alcohol-based slurry that is coated with the desired thickness onto a nickel screen, dried, and sintered. The dry-powder process covers the nickel screen with a prescribed thickness of dry nickel powder, which is directly sintered with no added pore-forming components.

All three of these processes have been used to produce sinter that has been used in well-performing nickel electrodes. Each process has also been used to produce sinter having a range of thickness and overall porosity. The thickness range of sinter made by these processes is typically 0.030 to 0.036 in., and the range of porosities typically available is 76–84%.

Sinter made by any of these three processes is generally controlled to produce a sintered sheet having both the desired thickness and overall porosity, as well as an adequate bend strength. Any internal variations in pore size or porosity are not tracked or controlled, but simply emerge as the consequences of that particular production process and its process controls. Here we have measured the variations in the internal pore characteristics of sinter made by all three processes. The objective of this study is to determine what, if any, systematic differences in the internal pore structure exist for nickel sinter made by each process.

2. Sinter Samples

A range of samples of various types of sintered-nickel plaque was obtained for this study. The samples are listed and described in Table 1. For each sinter sample obtained for analysis, two pieces were cut from different parts of the sample and analyzed separately. The A and B pieces are from one sinter sample, while the C and D pieces (or E and F pieces) are from additional sinter samples. Each piece of sinter used for the analysis was approximately 1 in. by 0.5 in. in size. Table 1 reports the measured thickness and porosity for each analysis piece. The nominal thicknesses are 30 mils for all the slurry samples (except 36 mils for 6A and 6B, and 33 mils for 6C and 6D), and 35 mils for all the dry-powder samples. The reported thickness measurements are the average of four measurements at different locations on each piece of sintered plaque. The nominal porosity is 76% for all slurry samples (except 78% for 6C and 6D) and 80% for all dry-powder samples. The reported porosity of each piece was determined from its volume (based on the measured thickness, length, and width of each piece) and weight, and assuming that it was composed of pure nickel metal.

Table 1. Sinter Samples Analyzed.

ID	Sample ID	Process	Thickness (mils)	Porosity (%)	Treatment
1A	4.5" coined sheet	Alcohol slurry	30.28	76.18	Oxidized
1B	4.5" coined sheet	Alcohol slurry	30.75	76.07	Oxidized
1C	3.5" coined sheet	Alcohol slurry	29.45	75.50	Oxidized
1D	3.5" coined sheet	Alcohol slurry	29.45	75.84	Oxidized
2A	L-439 C4	Alcohol slurry	31.50	76.02	Unoxidized
2B	L-439 C4	Alcohol slurry	30.51	75.53	Unoxidized
2C	L-439 C4	Alcohol slurry	31.69	76.27	Unoxidized
2D	L-439 C4	Alcohol slurry	30.67	75.66	Unoxidized
3A	L-438 C4	Alcohol slurry	29.65	76.09	Oxidized
3B	L-438 C4	Alcohol slurry	29.72	75.84	Oxidized
3C	L-438 C4	Alcohol slurry	29.41	76.02	Oxidized
3D	L-438 C4	Alcohol slurry	29.02	75.72	Oxidized
4A	L-0995	Dry powder	34.69	80.99	Unoxidized
4B	L-0995	Dry powder	34.72	81.16	Unoxidized
4C	L-0995	Dry -powder	34.45	80.72	Unoxidized
4D	L-0995	Dry powder	34.21	80.15	Unoxidized
5A	L-0992	Dry powder	36.10	81.95	Oxidized
5B	L-0992	Dry powder	35.63	81.52	Oxidized
5C	L-0992	Dry powder	34.96	80.79	Oxidized
5D	L-0992	Dry powder	34.92	80.99	Oxidized
6A	60-05-135-0	Aqueous slurry	37.95	77.99	---
6B	60-05-135-0	Aqueous slurry	35.78	76.59	---
6C	60-05-125-0	Aqueous slurry	34.45	78.90	---
6D	60-05-125-0	Aqueous slurry	32.83	78.59	---
6E	60-05-113-0	Aqueous slurry	31.10	76.63	---
6F	60-05-113-0	Aqueous slurry	31.18	76.76	---

The porosities reported in Table 1 include the nickel screen that is imbedded within the sinter as an electrically conductive supporting structure. If this supporting screen is not considered in determining the sinter porosity, a porosity for the sinter alone that is about 4% greater than that reported in Table 1 is obtained. The lower porosity that includes the screen is referred to as the plaque porosity, while sinter porosity refers to the sinter without the imbedded screen. All porosimetry measurements reported in the following sections refer to the sinter porosity, rather than the plaque porosity reported in Table 1.

3. Porosimetry Measurement and Analysis Method

The pores within each sample of sintered-nickel plaque were measured and analyzed using a method similar to the Scanning Porosimetry technique reported in Proc. of the 17th Annual Battery Conf. on Appl. and Adv.* Each sample was potted, cross-sectioned, and polished to enable high-quality images of the internal sinter to be obtained. However, rather than using piezoelectric positioners to automatically scan across the conductive features of the sinter as was done previously,* Scanning Electron Microscopy (SEM) images of the sinter were obtained that provided good contrast between the nickel sinter particles and the pores between the sinter particles. These SEM images were obtained with a resolution of 1 μm, with each image showing a 1200-μm length of the sinter sample. A typical SEM image is indicated in Figure 1. Approximately 20 non-overlapping images such as that indicated in Figure 1 were required to completely image all pores across the 1-in. length of each cross-sectioned sinter sample. In these SEM images, the nickel screen wires show up as large white circles or ellipses, the nickel sinter particles as small white regions, and the pores as dark regions that are surrounded by the sinter particles.

The method used to detect and measure the pores in each sinter piece involved scanning the pixels in a vertical line through the imaged cross-section of the sinter. A pore was detected and its size determined by the length of a dark segment of the line-scan, where the dark segment was terminated at each end by a region that was brighter than a threshold that was chosen for each image to discriminate between the nickel sinter and the void regions. This threshold was chosen to correspond to the mini mum in the distribution of pixel brightness that made up the image, as indicated in Figure 2 for a

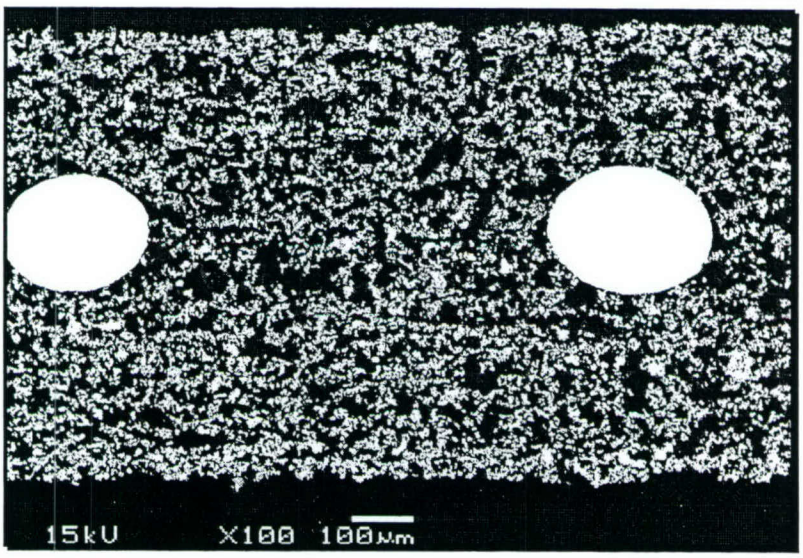

Figure 1. Typical SEM image of a cross-sectioned sinter sample.

* Zimmerman, A. H., G. A. To and M. V. Quinzio, *Scanning Porosimetry for Characterization of Porous Electrode Structures*, Proc. of the 17th Annual Battery Conf. on Appl. and Adv., IEEE 02TH8576, ISBN 0-7803-7132-1, 2002, pp. 293-298.

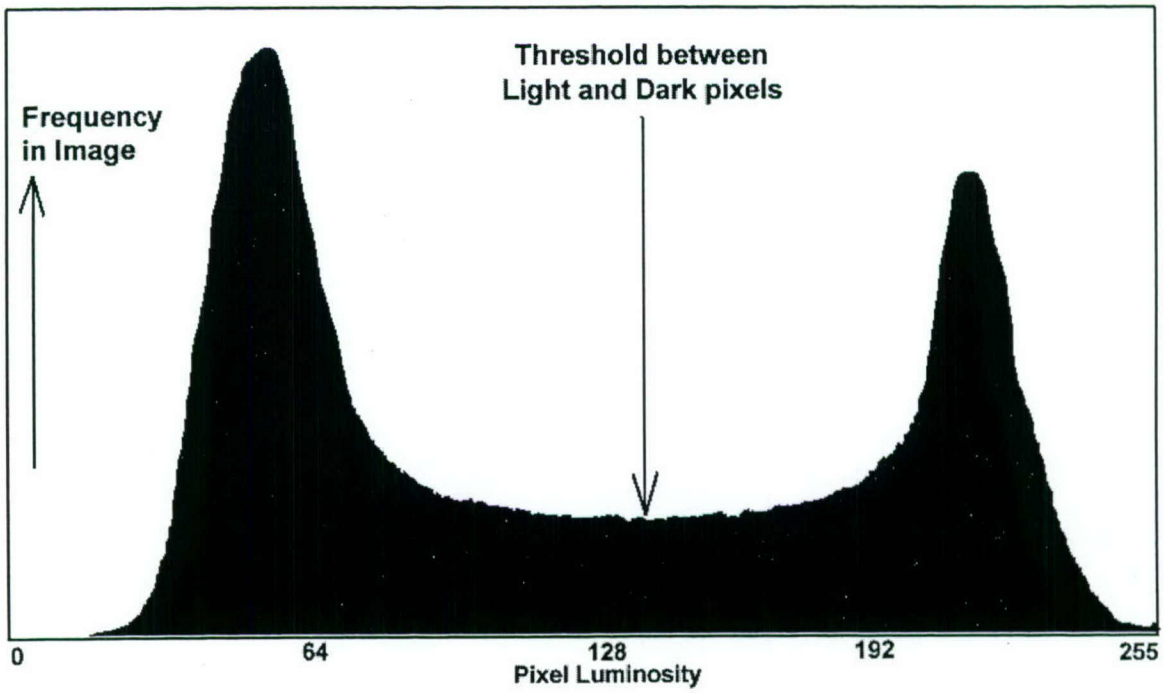

Figure 2. Distribution of the pixel luminosity over a typical 1200- by 960-μm SEM image of a cross-sectioned nickel sinter sample.

typical sample. Because the pixels in each image have a 1-μm resolution, the boundaries between sinter particle and void could be determined to 0.1-μm precision by interpolation of the intensity gradients between adjacent pixels. While the procedure did not allow pores smaller than 0.5 μm in diameter to be detected, it did enable the size of the pores that are detected to be determined to ±0.2 μm precision.

The line-scans that were applied to a sinter image such as shown in Figure 1 were spaced such that adjacent scans would not pass through the same circular void regions, thus avoiding the possibility of counting large pores twice during adjacent scans. This requirement led to significantly greater spacing between adjacent line-scans when large pores were detected, than when the pores were smaller. In addition, the line scans were located so that they did not pass through any of the large grid wires shown in Figure 1, which have zero porosity.

The one-dimensional line-scan method used to detect pore sizes as described above assumes that the pores are randomly oriented and have random shapes. Examination of images such as those shown in Figure 1 suggest that this is true for the most part, although occasionally long horizontal voids are seen. With the line-scan method used here, a long horizontal void would be counted as a chain of nearly circular pores having a diameter equal to the vertical width of the void. No preferentially vertical-oriented voids (vertical cracks) were seen in any of these sinter samples.

Approximately 320 line-scans were carried out over the 20–21 images that spanned the 1-in.-long cross-sectioned sample. These scans typically detected 12,000 to 20,000 pores of various sizes ranging from 0.5 μm to over 100 μm in diameter. These pores were sorted into 5 bins that corresponded

to different locations through the thickness of the sinter. Bins 1 and 5 corresponded to the surface regions on each side of the sinter, while bin 3 corresponded to the center of the sinter. The location of the center of each pore dictated the bin into which it was placed. These five bins thus provide an indication of how uniform the pore characteristics are through the thickness of the sinter. The distribution of average pore size, average porosity, or pore uniformity through the sinter thickness can be readily examined, along with the changes in the pore size distribution through the sinter.

4. Unique Sinter Structures

A number of unusual or unique structural features were seen when analyzing the SEM images during this study. The sinter shown in Figure 1 is typical of a relatively uniform and desirable structure. The types of departure from this relatively uniform structure, which are in some cases key factors in dictating the porosity characteristics, can be classified into either abnormal voids or abnormal nickel aggregates. Each of these types of features will be shown and discussed here, along with an indication of what types of sinter showed each condition and how frequently it was seen.

4.1 Unusual Sinter Voids

The type of void that was most often found to strongly influence the pore size distribution was the large internal void. These types of voids were seen exclusively in slurry sinter, and were seen with much greater frequency in the alcohol-based slurry sinter. These voids may be classified as voids associated with central grid wires in the sinter, or large voids away from the center of the sinter and its supporting grid structure. The former type of void is shown in Figure 3, while the latter type is shown in Figure 4.

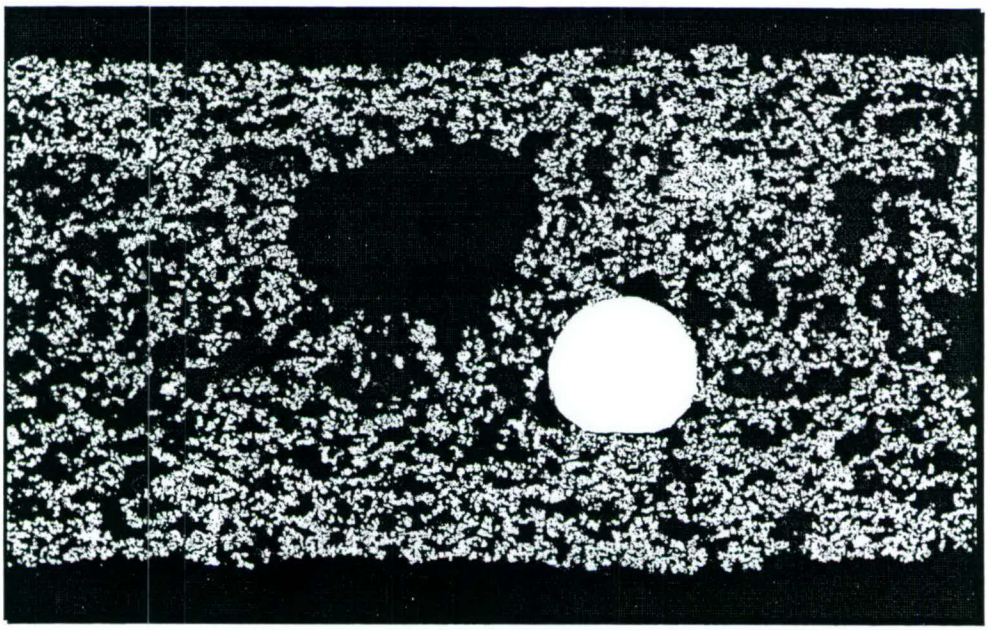

Figure 3. Large void frequently seen in alcohol-based slurry sinter away from the center grid-containing region.

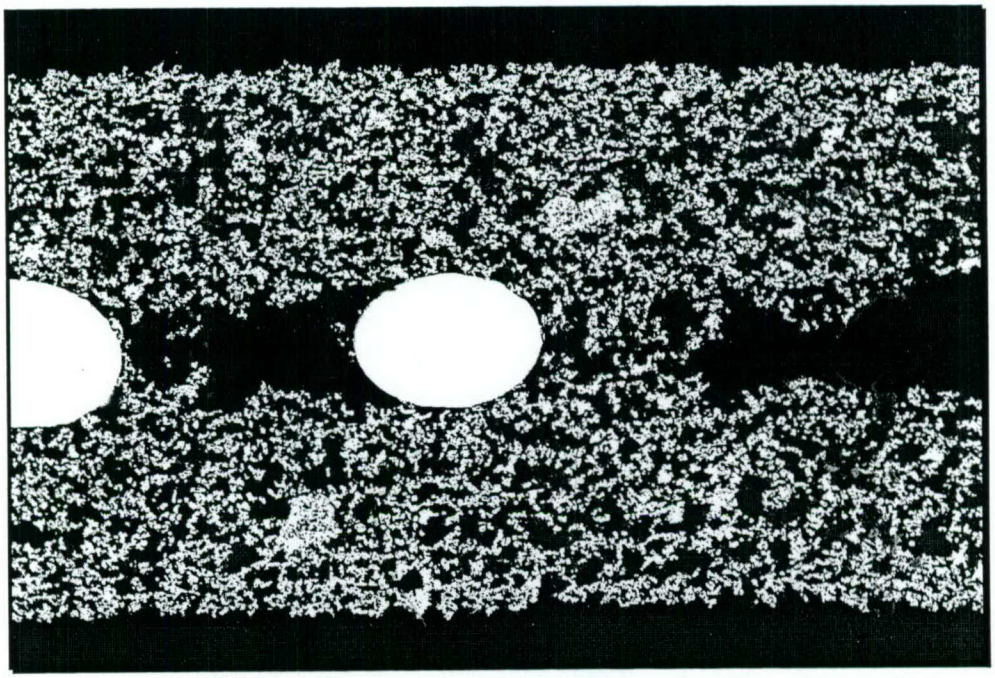

Figure 4. Large voids frequently seen in alcohol-based slurry sinter in proximity with the center grid wires.

The large voids shown in Figures 3 and 4 are particularly undesirable because if they are loaded with nickel electrode active material, the active material is not very well utilized for storing energy because of the large distance through the active material to the nearest conductive metal surfaces. If the voids are not loaded with active material, the sinter must be over-loaded elsewhere to provide the correct average amount of active material. Typically, nickel electrodes made from sinter having large internal voids exhibit a significantly lower utilization than can be obtained with a uniform sinter. The large voids can also act as stress points within the finished nickel electrode where blisters can form or the sinter can delaminate from the grid after long-term electrode operation. In several instances, the large voids seen in Figure 4 appeared to be reduced in thickness to where the void appeared more as a crack along the center line where the grid wires were situated in the sinter, as shown in Figure 5.

Voids within the sinter were also seen in dry-powder sinter, although these voids typically had a different appearance than those in slurry sinter (Figures 3 through 5). In dry sinter the most common type of void is seen immediately around a portion of the grid wires, where it appears that the nickel powder separated from the grid wire prior to or during the sintering operation. This type of void is shown in Figure 6. While this kind of void tends to cause the same type of reduced nickel electrode utilization that large voids cause in slurry sinter, it can provide an oxygen flow path from the interior of the nickel electrode to the outer surface. In dry-powder sinter, the grid wire structure is generally situated at one edge of the sinter, thus any significant voids around these grid wires are often open to the electrode surface, as is the case in Figure 6. One can often visually see the exposed grid wires through such voids on the surface of the sinter. This type of surface void is why the screen side of dry-powder sinter is positioned so that it does not face the separator in nickel-hydrogen cells.

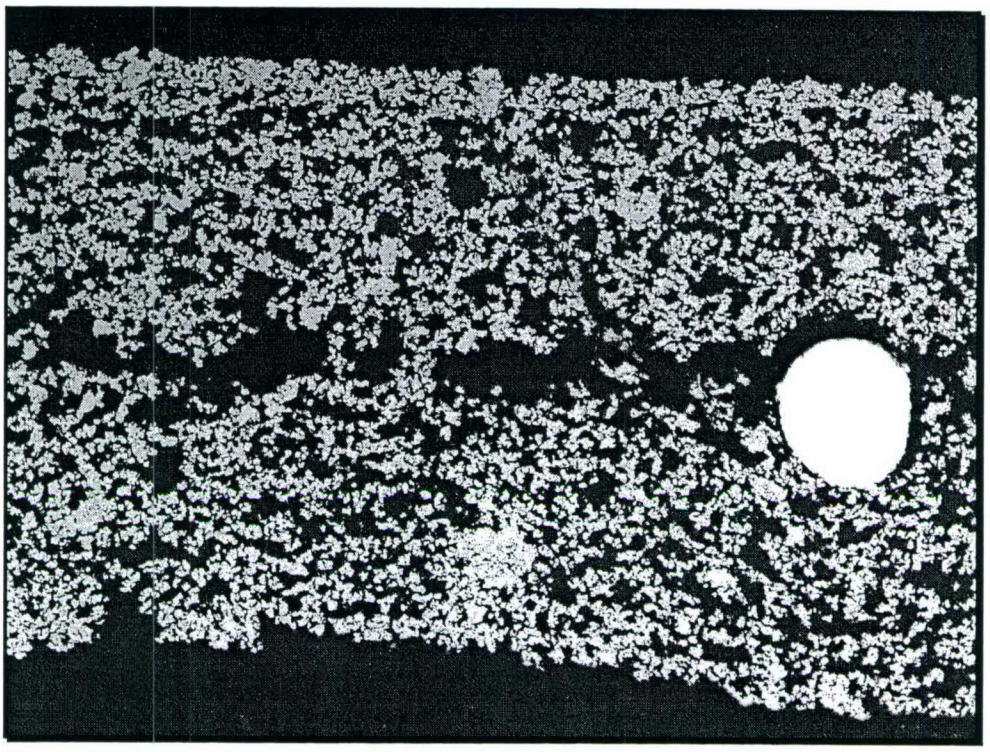

Figure 5. Center void that has thinned down to appear more like a crack that is occasionally seen in slurry sinter.

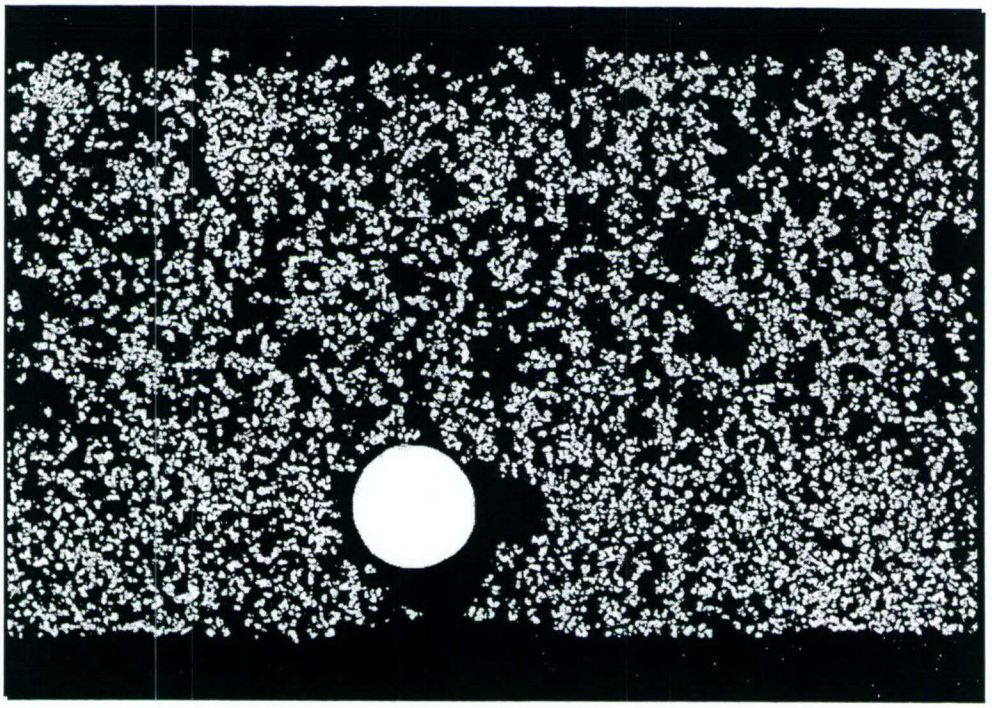

Figure 6. Void commonly seen in dry-powder nickel sinter where the powder has separated from the grid wires.

The second type of void that is occasionally seen in dry-powder sinter is a crack in the sinter, an example of which is shown in Figure 7. These cracks appear in most instances to have formed before the powder was sintered since there is no evidence of actual breaking of the necks between the sinter particles, and is probably caused by movement of the powder layers prior to sintering. These cracks can act as stress points where blisters form in finished nickel electrodes.

4.2 Unusual Sinter Aggregates

In addition to voids in nickel sinter, undesirable aggregates of nickel powder are also sometimes seen. The most common type of aggregate is a region of high-density nickel powder imbedded within the sinter. An example is shown in Figure 8 for an alcohol-based slurry sinter sample, which is the type of sinter that most commonly displays this type of aggregate. Aggregates of this type were much less common in the waster-based slurry sinter samples, and when seen tended to be significantly smaller than those shown in Figure 8. Aggregates of the type shown in Figure 8 mean that there are lower density regions elsewhere in the sinter if it is manufactured to the required overall porosity. The lower density regions (which often include larger voids) will tend to be loaded with more active material than the high-density regions shown in Figure 8, but will have lower utilization and thus reduce the overall utilization of the nickel electrode. One unusual aggregate was seen protruding from the surface of a water-based slurry sinter sample, as shown in Figure 9. A protruding aggregate of this type is a concern because it can cause a stress point on the separator in a nickel-hydrogen cell stack, potentially increasing the probability of separator damage and the formation of a short circuit.

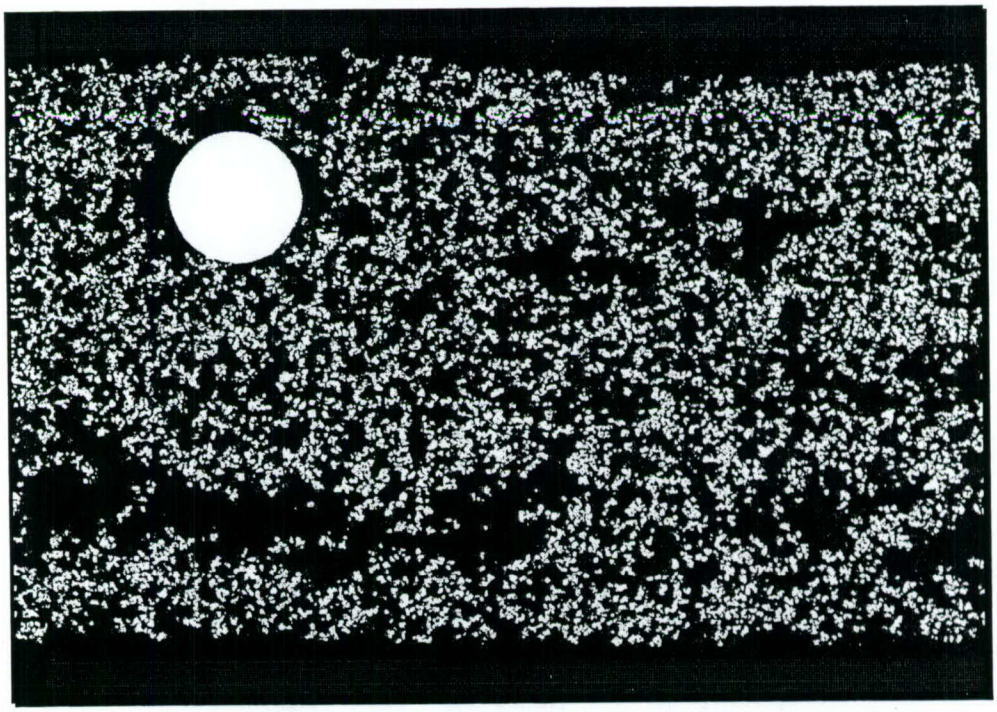

Figure 7. Horizontal crack or void occasionally seen on the side of dry-powder sinter where there are no supporting grid wires.

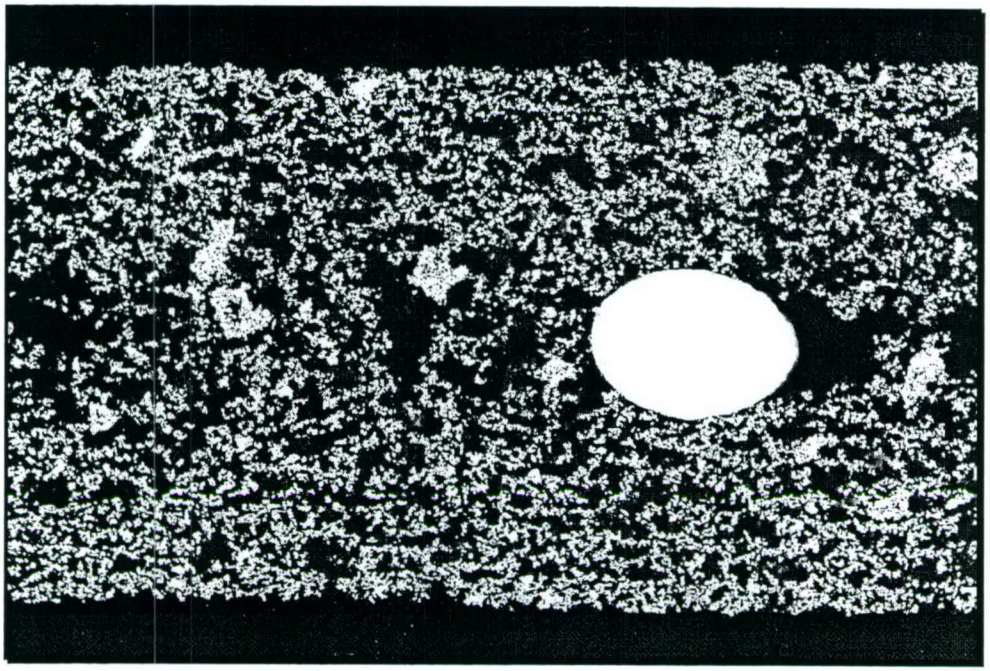

Figure 8. High-density aggregates of nickel powder frequently seen in alcohol-based slurry nickel sinter.

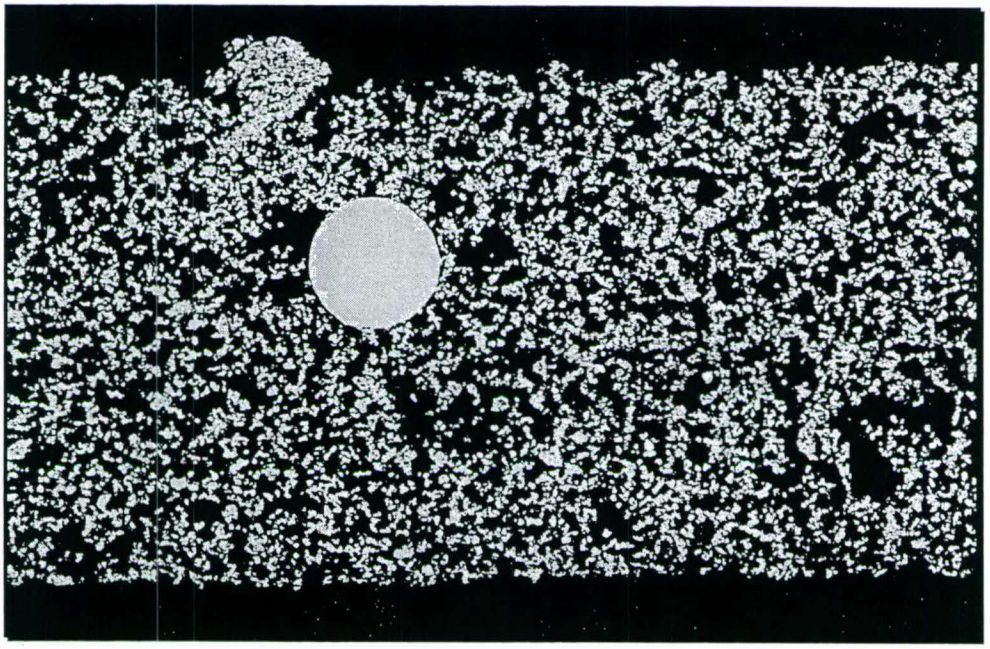

Figure 9. Surface aggregate or lump of high-density nickel powder seen infrequently (once) for water-based slurry nickel sinter.

Aggregates of nickel in dry-powder sinter have a quite different appearance than those illustrated in Figures 8 or 9. The most common type of aggregate in dry-powder sinter is an extended chain of nickel particles that have been sintered into loops having either open (most common) or closed geometry. An example of a closed-loop aggregate is shown in the bottom-center region of Figure 10. While these chains and looped chains of sinter can be as large as 50 μm in size, they are not expected to have a significant effect on the performance of the dry-powder sinter because they do not appear to significantly alter the sizes or distributions of pores within the sinter.

An example of an unusual aggregate was observed in a sample of dry-powder sinter. This aggregate appeared as a needle-like particle of solid nickel metal, and is shown in the bottom-center region of Figure 11. It is not clear whether this was a large pre-sintering fragment of metal, or whether it is simply a mass of smaller particles that were melted into a larger particle having a quite unusual and regular shape.

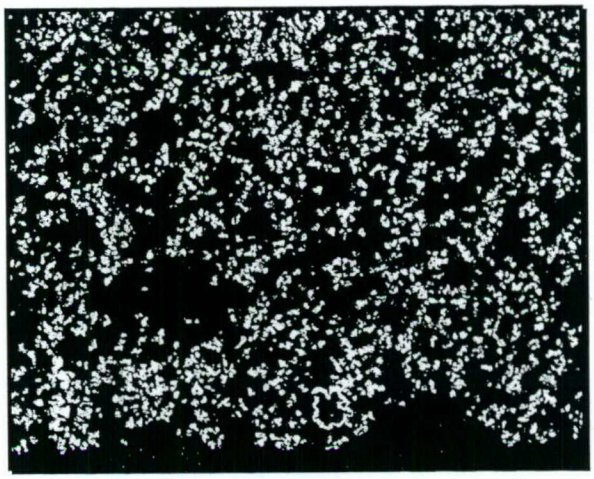

Figure 10. Nickel particles sintered into a closed-loop chain in a dry-powder sinter sample.

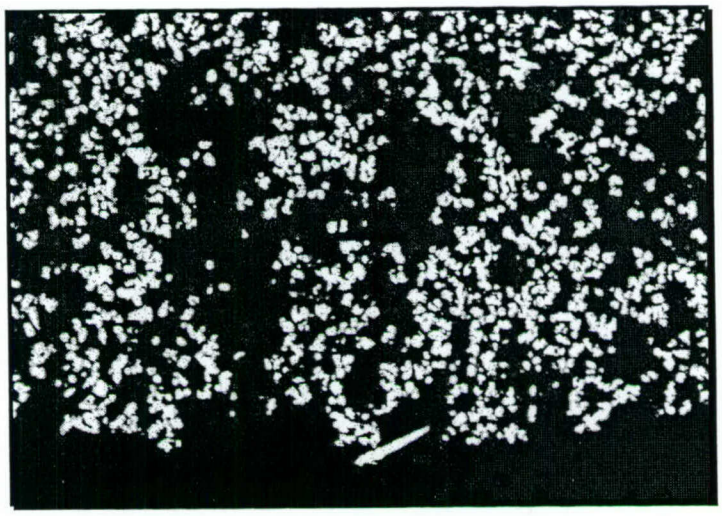

Figure 11. Needle-shaped nickel fragment seen in one sample of dry-powder nickel sinter.

5. Porosimetry Results

The porosimetry analysis described in Section 3 results in distributions of pore volume as a function of pore size within each of the five regions through the thickness of each sinter sample. These pore size distributions reveal how the internal pore volume is distributed between differing types of pores in the samples. It is possible that some regions can exhibit bi-modal size distributions, while others can exhibit distributions where the pore volume is mostly in a few large voids, while other samples may exhibit quite uniform distributions throughout their thickness. In general, it is desirable to have relatively uniform distributions of pore volume. In addition, the average pore size and the average sinter porosity may be determined from the pore size distributions through the thickness of each sinter sample. In this section, the detailed results of the porosimetry results obtained here are described for the alcohol-based slurry sinter, the water-based slurry sinter, and the dry-powder sinter.

5.1 Alcohol-Based Slurry Sinter

As indicated in Table 1, twelve samples of alcohol-based slurry sinter were analyzed. The typical variation in pore size distribution through the thickness of these samples is shown in Figure 12. The most noteworthy characteristic of these distributions is the large increase in the pore sizes toward the center of the sample. This change is entirely due to the large voids seen in this type of slurry, and which are illustrated in Figures 3 and 4.

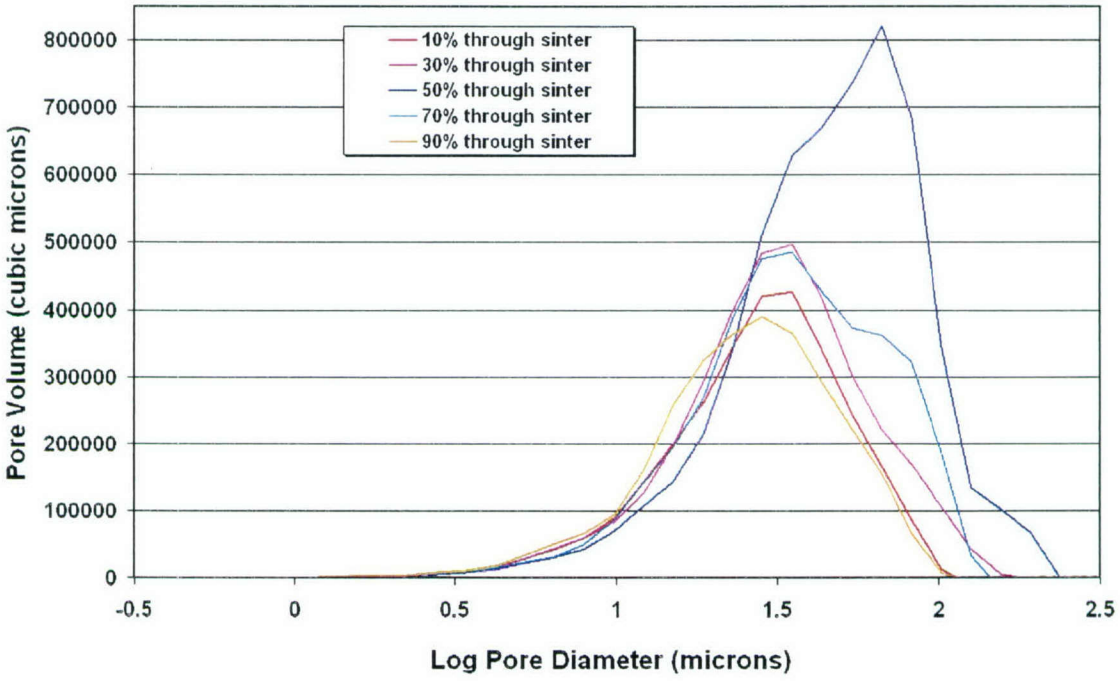

Figure 12. Changes in the pore size distribution through the thickness of a typical sample of alcohol-based slurry sinter. These data are from sample 2D.

The changes in the pore size distributions are more easily compared for the different sinter samples by plotting the average pore size and the average sinter porosity as a function of the sinter thickness. These plots are shown in Figures 13 through 18 for the alcohol-based slurry sinter samples in Groups 1 through 3.

The most significant variation in pore characteristics in these alcohol-based slurry samples is the large average pore size at the center of the plaque in many (but not all) of the samples analyzed. This peak arises from the large voids that frequently are seen at the center of the sinter, often in association with the location of the nickel screen wires. These voids are, however, not always present, as can be seen in Figure 15 where only one of the pieces cut from each sinter sample had the large internal voids. In the areas where the large internal voids were detected, the average pore size near the center of the sinter exceeded 80 μm, while in the areas that did not display the large internal voids the average pore size near the center of the sinter was about 45 μm. While these variations in internal pore size are likely to cause a noticeable decrease in the utilization of nickel electrodes made from this sinter, historically slurry sinter that contains large internal voids has been used to produce acceptably performing nickel electrodes.

The average porosity of the sinter samples in these three groups shows several features of interest. First, the samples having large internal voids also have a peak in the average porosity that results from the large voids. This is an expected result from the non-uniform porosity that is caused by the large voids. The second signature, which is characteristic of slurry sinter in general, is the decrease in average porosity at the surfaces of the sinter. Slurry sinter always seems to have a "skin" of higher density sinter at its surfaces. This characteristic lends it some added strength, and can also act to prevent active material from being easily extruded from the pores at the "skin" of the sinter.

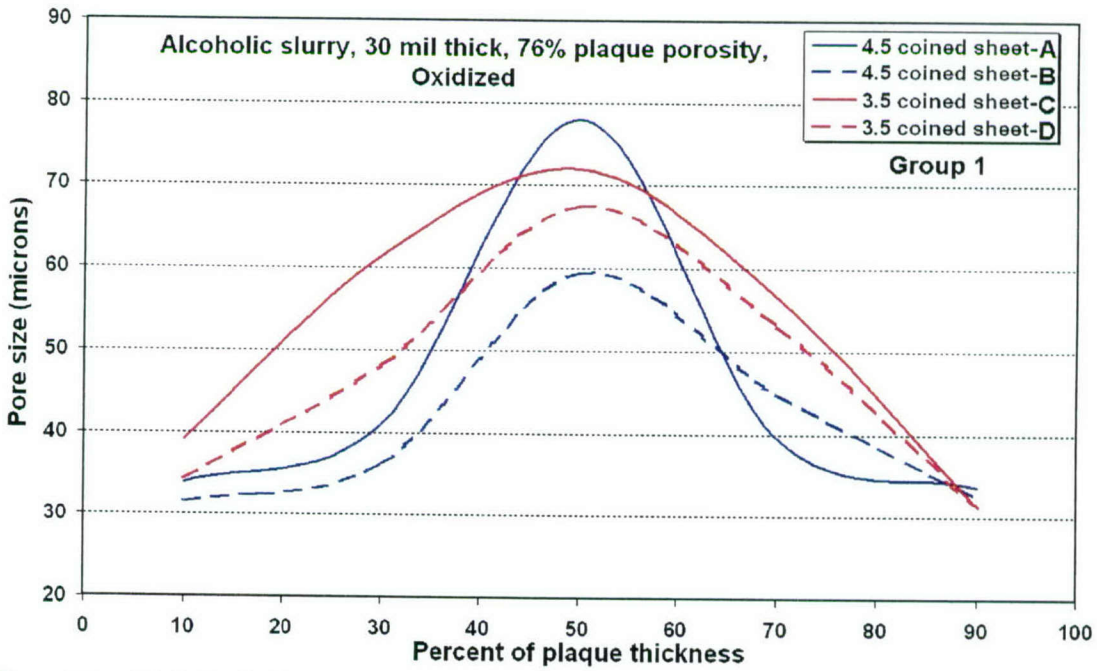

Figure 13. Variation in the average pore size through the thickness of alcohol-based slurry sinter samples from Group 1.

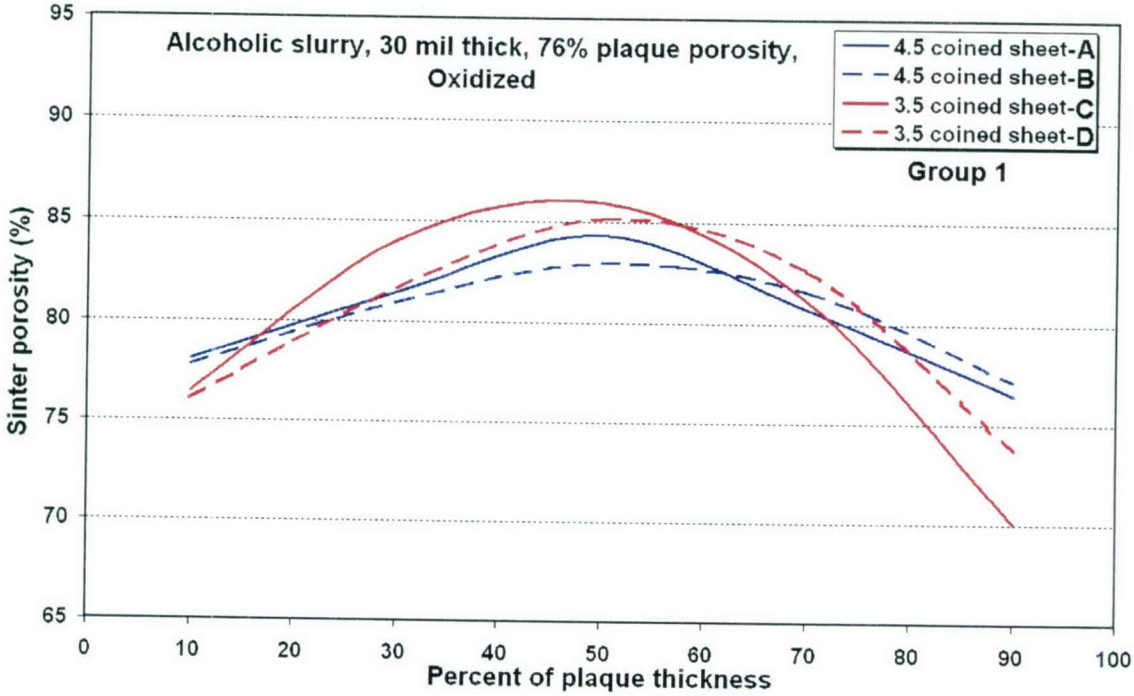

Figure 14. Variation in the average sinter porosity through the thickness of alcohol-based slurry sinter samples from Group 1.

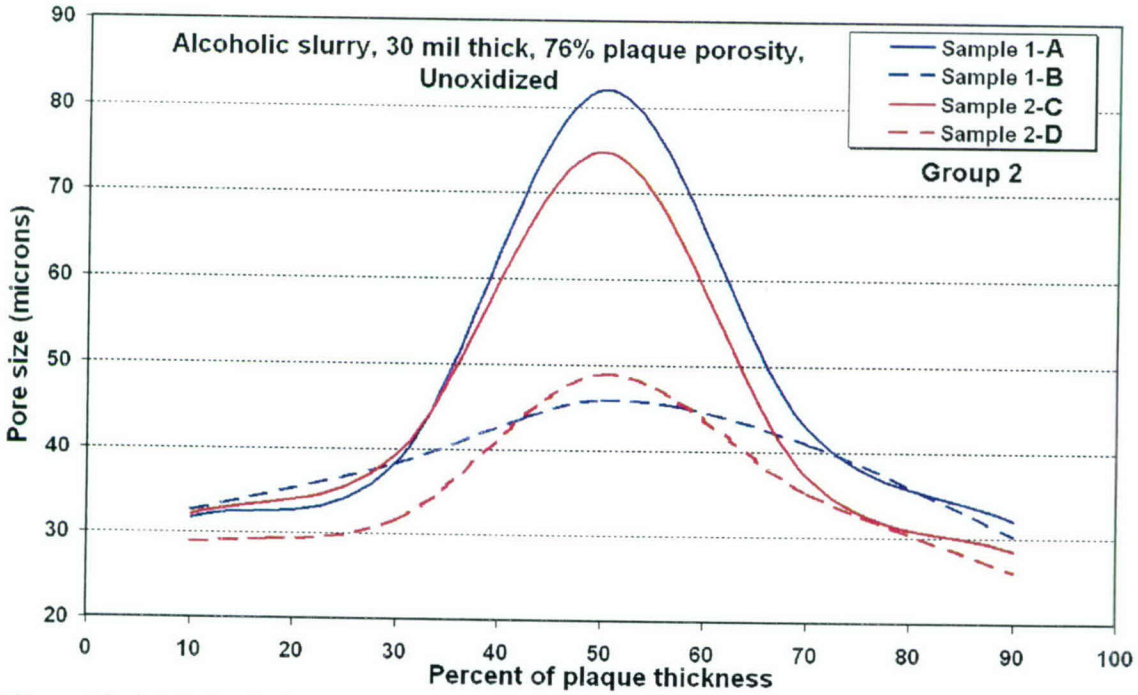

Figure 15. Variation in the average pore size through the thickness of alcohol-based slurry sinter samples from Group 2.

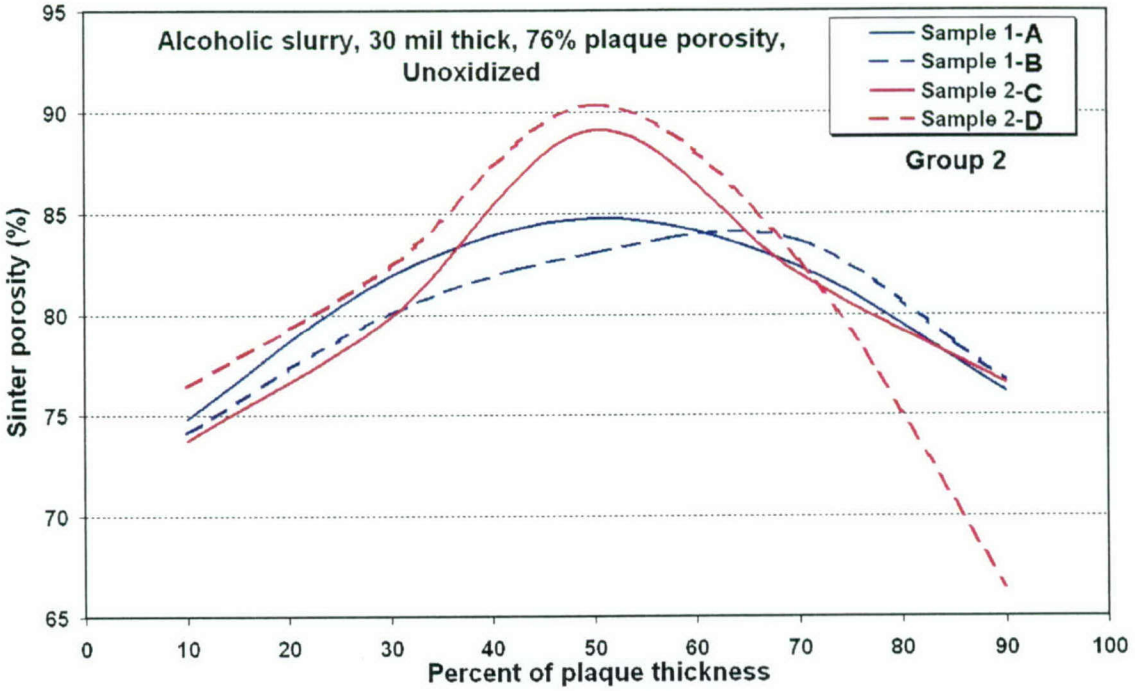

Figure 16. Variation in the average sinter porosity through the thickness of alcohol-based slurry sinter samples from Group 2.

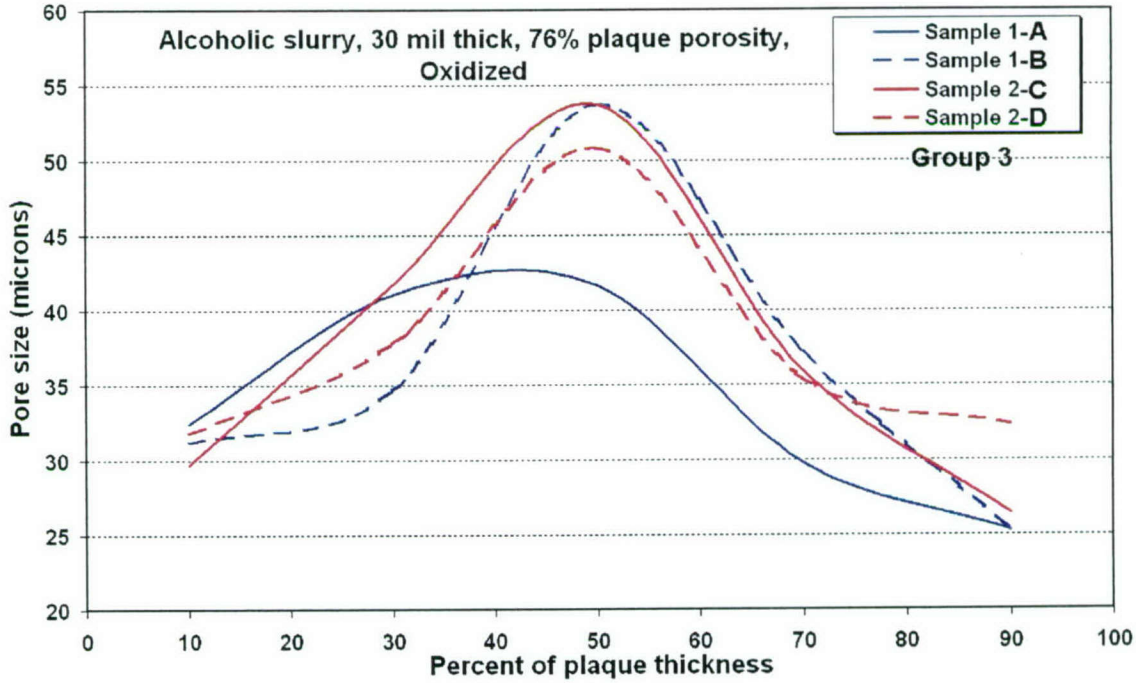

Figure 17. Variation in the average pore size through the thickness of alcohol-based slurry sinter samples from Group 3.

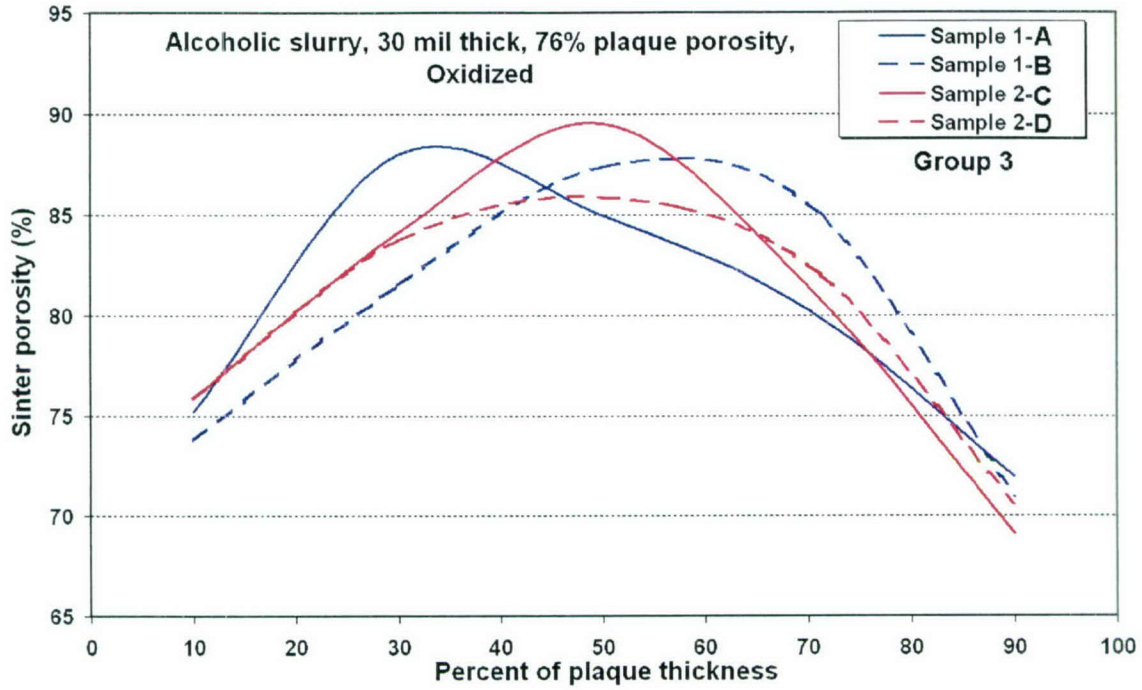

Figure 18. Variation in the average sinter porosity through the thickness of alcohol-based slurry sinter samples from Group 3.

These results suggest that alcohol-based slurry sinter plaques of the types analyzed here consist of a composite of many regions containing large internal voids and some other regions containing a relatively uniform pore distribution through the plaque thickness. In the regions with large voids, the average pore size can exceed 80 μm at the center of the plaque. In the regions with uniform pore size distributions, the pore sizes typically range from 25 to 45 μm through the thickness of the plaque.

Comparison of the oxidized to the un-oxidized plaque samples indicated that the oxidation process did not significantly affect the porosity or pore size characteristics.

5.2 Water-Based (Aqueous) Slurry Sinter

As indicated in Table 1, six samples of water-based slurry sinter were analyzed. The typical variation in pore size distribution through the thickness of these samples is shown in Figure 19. In this figure, the sinter appears to consist of two overlapping distributions. A sub-distribution peaking at about 35 μm appears to correspond to a uniform distribution that exists in the outer layers and in about 50% of the central volume of the plaque. A second sub-distribution peaking at about 50–60 μm appears to coincide with larger pores or voids in the center of the sinter. These larger pores are much smaller than the 100–140 μm voids seen in alcohol-based slurry sinter, and also appear to follow a statistically discrete distribution function.

The changes in the pore size distributions are more easily compared for the different sinter samples by plotting the average pore size and the average sinter porosity as a function of the sinter thickness. These plots are shown in Figures 20 and 21 for the water-based slurry sinter samples in Group 6.

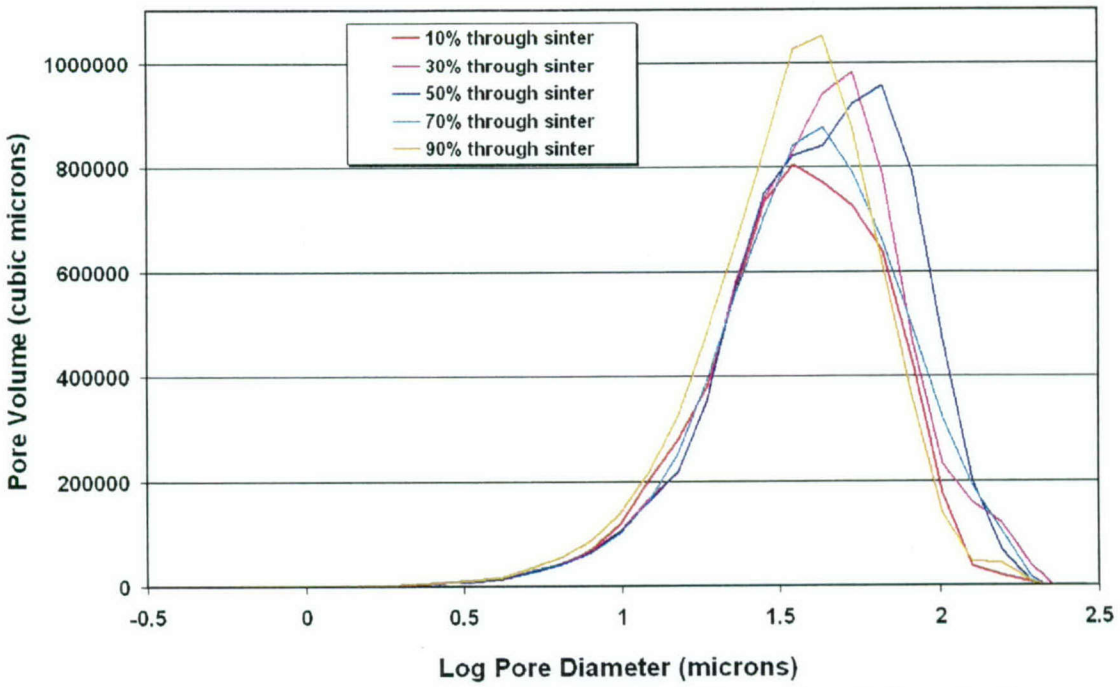

Figure 19. Changes in the pore size distribution through the thickness of a typical sample of water-based (aqueous) slurry sinter. These data are from sample 6D.

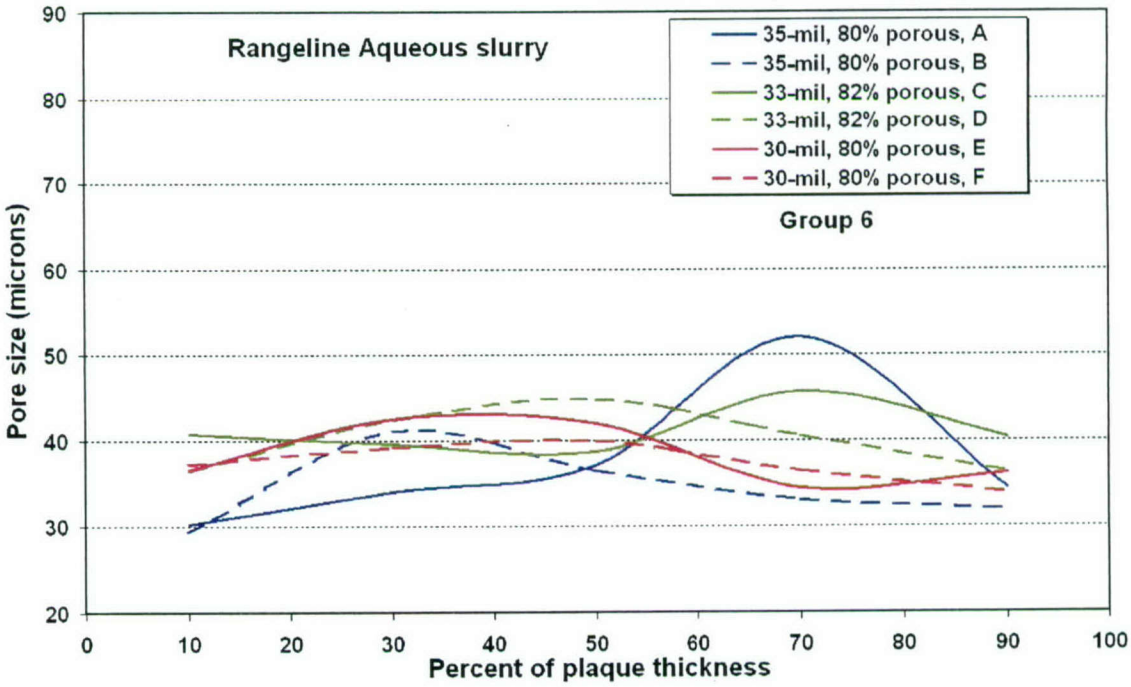

Figure 20. Variation in the average pore size through the thickness of water-based (aqueous) slurry sinter samples from Group 6.

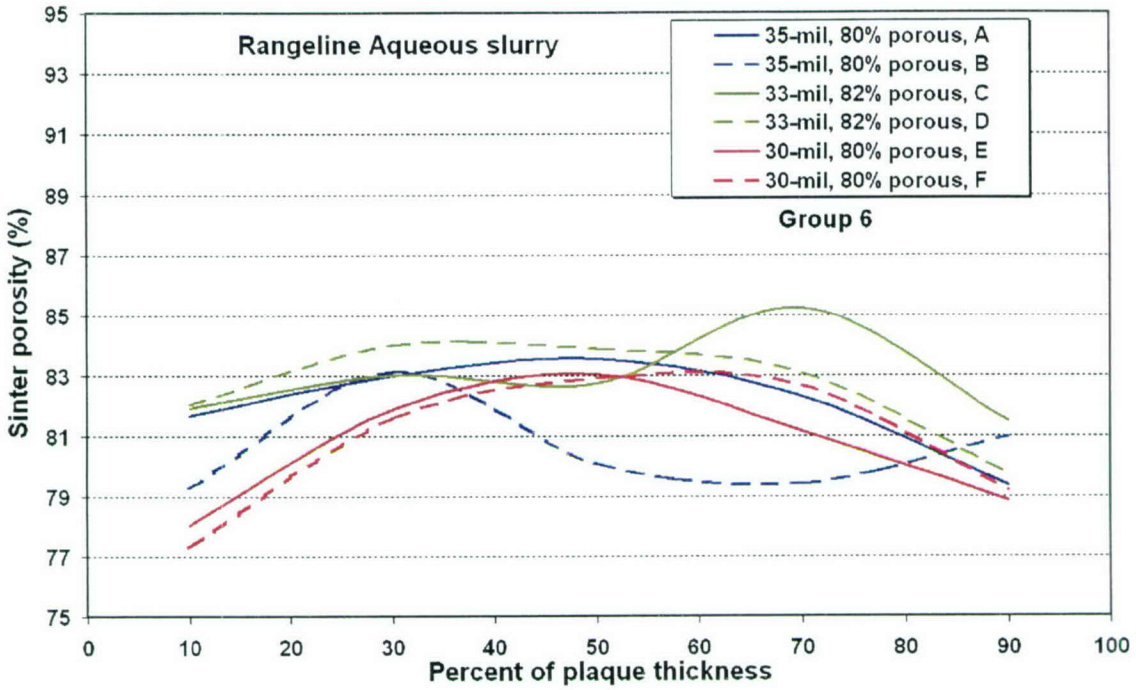

Figure 21. Variation in the average sinter porosity through the thickness of water-based (aqueous) slurry sinter samples from Group 6.

In comparison with the alcohol-based slurry samples, the water-based slurry appears to be much more uniform through its thickness, both in terms of the pore size and the sinter porosity. It still exhibits the more dense "skin" that is generally associated with slurry sinter; however, the porosity increases at this "skin" are less pronounced. One sample (6C) displayed peaks in both the porosity and pore size that correspond to some small voids about 70% through the thickness of this piece.

The sinter samples from the aqueous slurry process included samples of three differing thicknesses and two differing average porosities, yet no real systematic variations in either pore size or sinter porosity are seen in response to these process changes. This apparent insensitivity of the pore characteristics to intentional process changes suggests that the process controls are relatively robust for making this type of sinter.

5.3 Dry-Powder Sinter

As indicated in Table 1, eight samples of dry-powder sinter were analyzed. The typical variation in pore size distribution through the thickness of these samples is shown in Figure 22. In this figure, the sinter consists of two overlapping distributions. A sub-distribution peaking at about 35 μm appears to correspond to a uniform distribution that exists to some degree in all regions through the plaque. A second sub-distribution peaking at about 60 μm appears to coincide with larger pores in the sinter. The peak at about 85 μm in the distribution 90% of the way through the sinter is largely caused by the voids around the grid wires that are illustrated in Figure 6. If these grid-wire voids are ignored, the pore distributions for dry sinter are remarkably similar to those of aqueous slurry sinter.

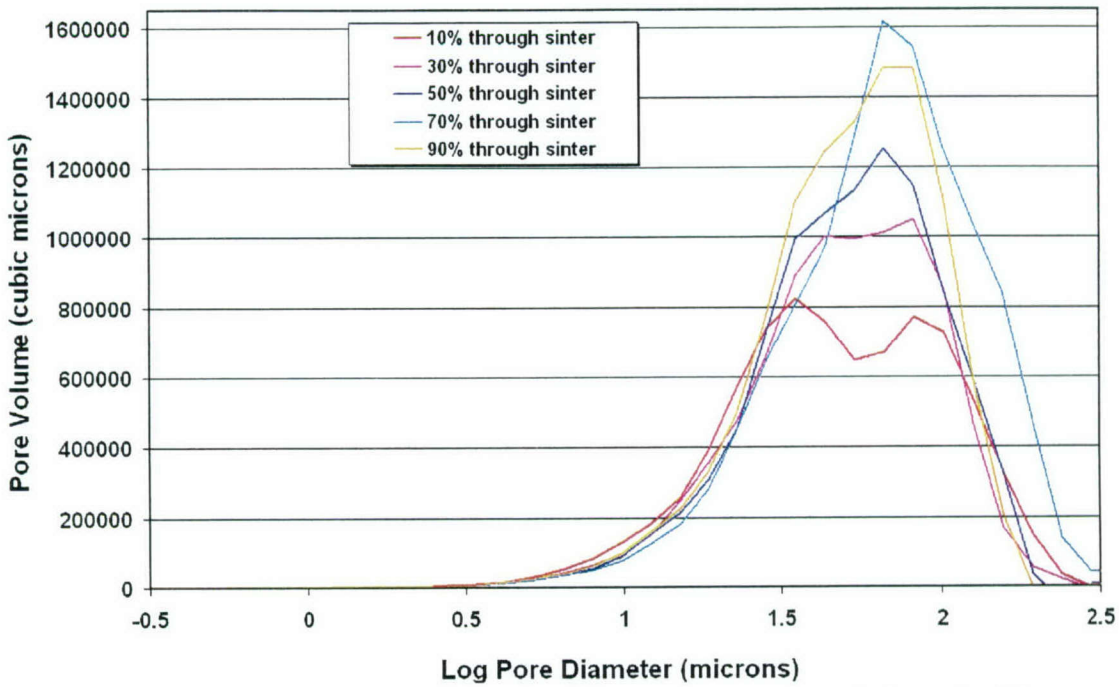

Figure 22. Changes in the pore size distribution through the thickness of a typical sample of dry-powder sinter. These data are from sample 4A.

The changes in the pore size distributions are more easily compared for the different sinter samples by plotting the average pore size and the average sinter porosity as a function of the sinter thickness. These plots are shown in Figuress 23 through 26 for the dry-powder sinter samples in Groups 4 and 5.

The pore sizes for the dry-powder sinter range from 40 to 70 μm through the thickness of the samples. These pore sizes are generally larger than for the regions in slurry sinter that do not contain large voids, whether alcohol or water based. Because the dry-powder plaque has its internal nickel-supporting screen on one side, the plaque has intrinsic gradients through its thickness. The screen side can have a somewhat denser sinter because the nickel powder settles slightly before it is sintered. However, this effect can be offset by voids that can form around the grid wires. When these effects are combined with some compression of the skin of the sinter that is often seen, the result can be two peaks in the sinter porosity, one on the screen side and one on the other side. This behavior can be seen in Figures 24 and 26.

While the pore sizes within dry-powder sinter are seen to vary in the 40–70 μm range, there is not an extremely large variation in the average sinter porosity. The densest "skin" regions of the dry-powder sinter drop to 80–81% porosity, which is only 3–4% lower than the nominal overall plaque porosity. Similarly, the most porous interior regions of the dry-powder sinter rise to 88–89% porosity, which is only 4–5% higher than the nominal overall plaque porosity. It can be noted by examination of Table 1 that most of these dry-powder sinter samples had an overall plaque porosity about 1% greater than the nominal 80% porosity expected for this type of dry-powder sinter.

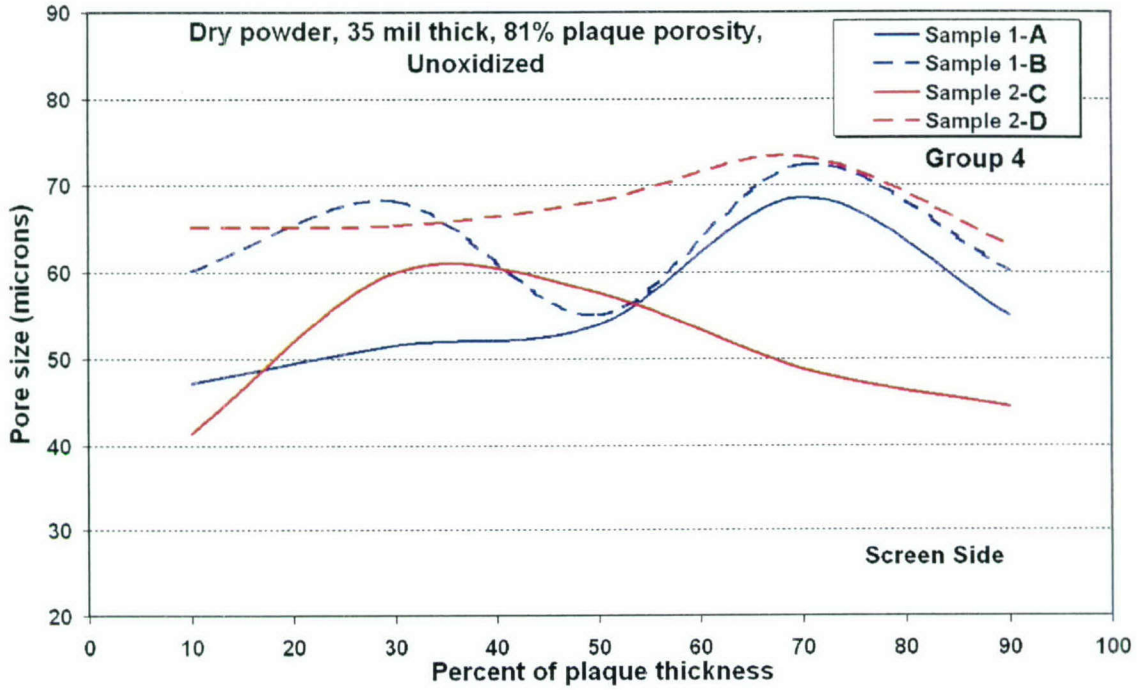

Figure 23. Variation in the average pore size through the thickness of dry-powder sinter samples from Group 4.

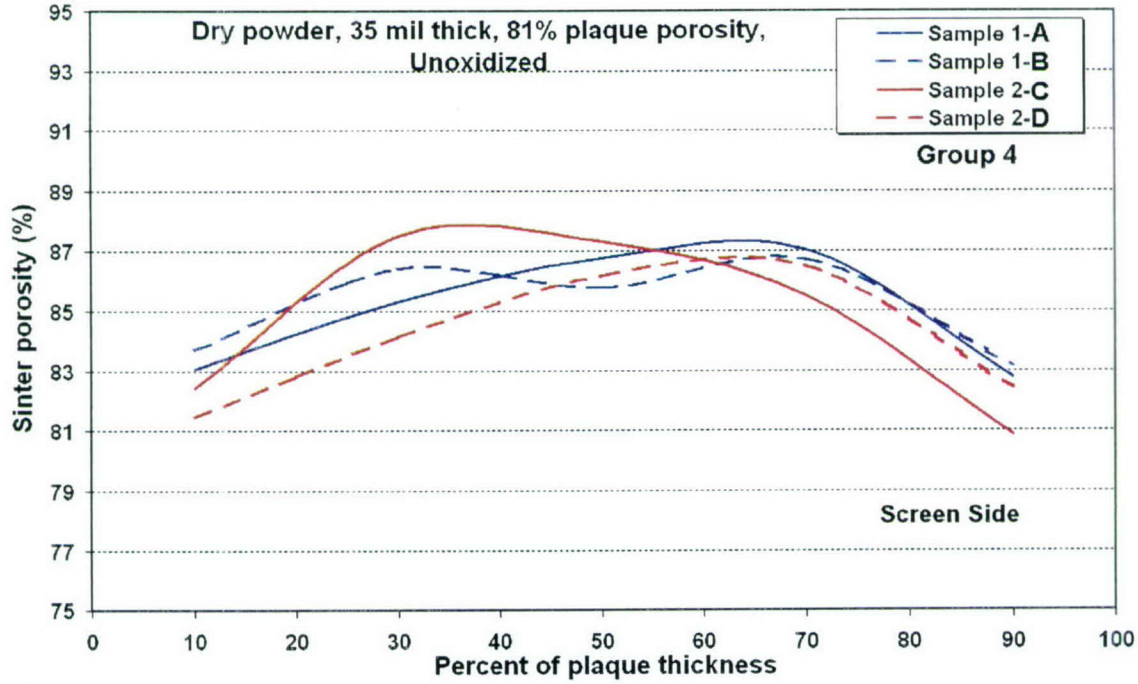

Figure 24. Variation in the average sinter porosity through the thickness of dry-powder sinter samples from Group 4. The overall sinter porosity in these samples is nominally 84%.

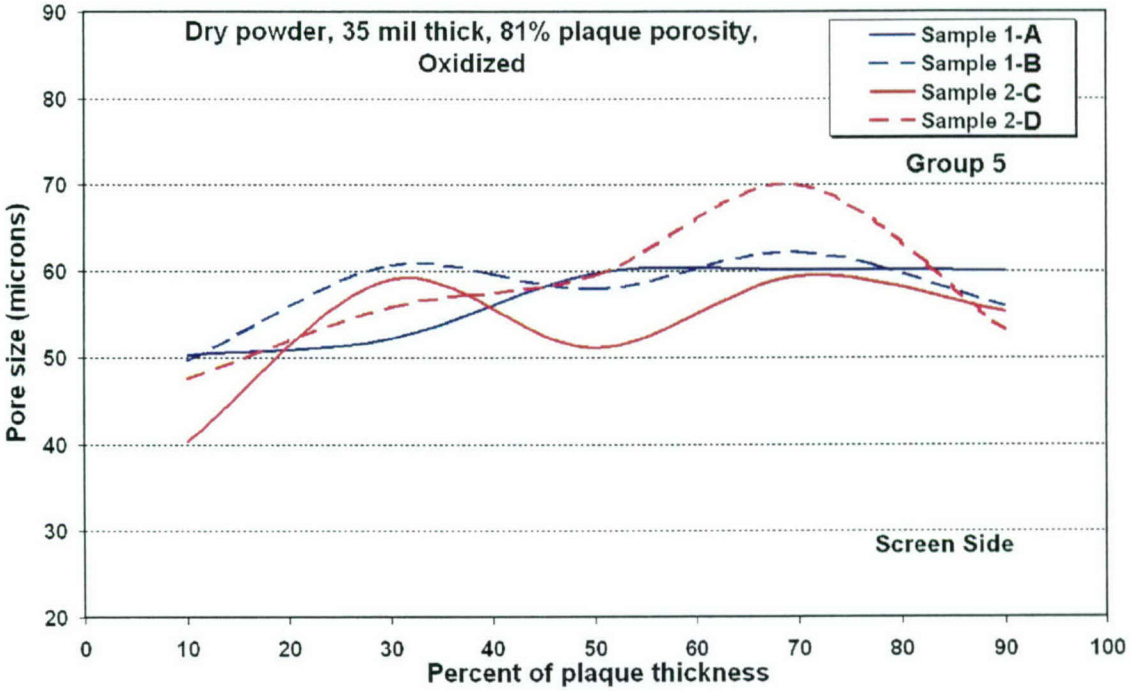

Figure 25. Variation in the average pore size through the thickness of dry-powder sinter samples from Group 5.

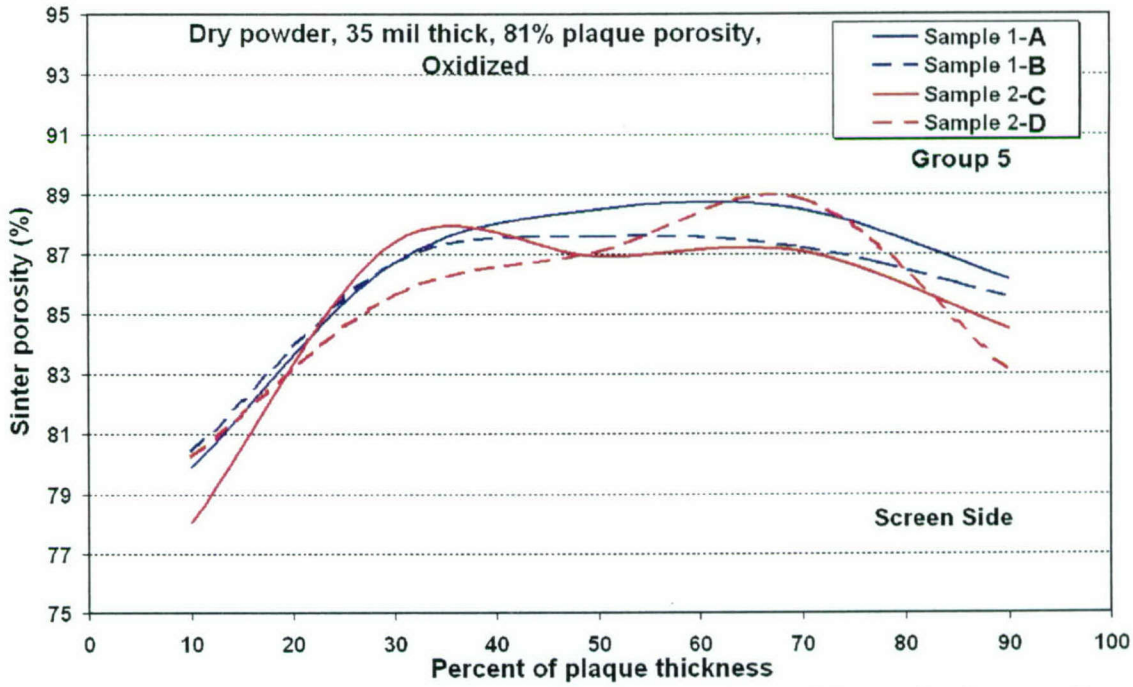

Figure 26. Variation in the average sinter porosity through the thickness of dry-powder sinter samples from Group 5. The overall sinter porosity in these samples is nominally 84%.

6. Discussion of Results

Each of the three types of sinter analyzed here displays some unique signatures in terms of the pore size distributions, as well as their uniformity through the thickness and over the surface of the sintered plaque samples.

The alcohol-based slurry plaque displays pore distributions that are dominated by large internal voids combined with regions of highly densified sinter. These highly non-uniform regions of sinter occur in more than 50% of the plaque samples analyzed; however, a number of regions containing much more uniform distributions of pore sizes were also observed. Thus, the pore characteristics of the alcohol-based slurry plaque and the other types of sinter studied here are probably best evaluated based on the uniformity of the pore distribution through the plaque thickness from sample to sample.

Evaluation of pore uniformity was made by expressing the range of observed pore sizes or porosity through the thickness of all samples from each sinter group as a percentage of the overall average pore size or porosity. Pore variability or uniformity expressed in this manner is indicated in Figures 27 and 28Figure 27 graphically shows that pore size uniformity is poor and highly variable in the alcohol-based slurry, while the dry sinter and water-based slurry sinter have considerably less pore size variability. Figure 28 graphically illustrates that the alcohol-based slurry also has much greater variability in its porosity, while the dry sinter and water-based slurry sinter have a much more uniform sinter porosity.

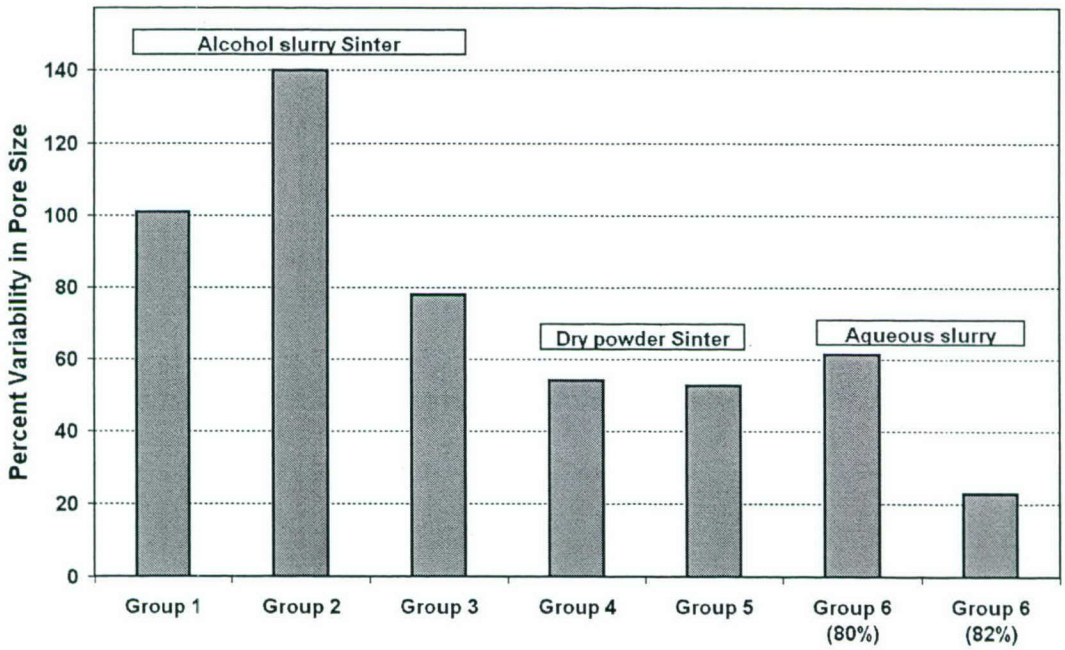

Figure 27. Variability in pore size (as a percentage of overall average pore size) for each type of sinter.

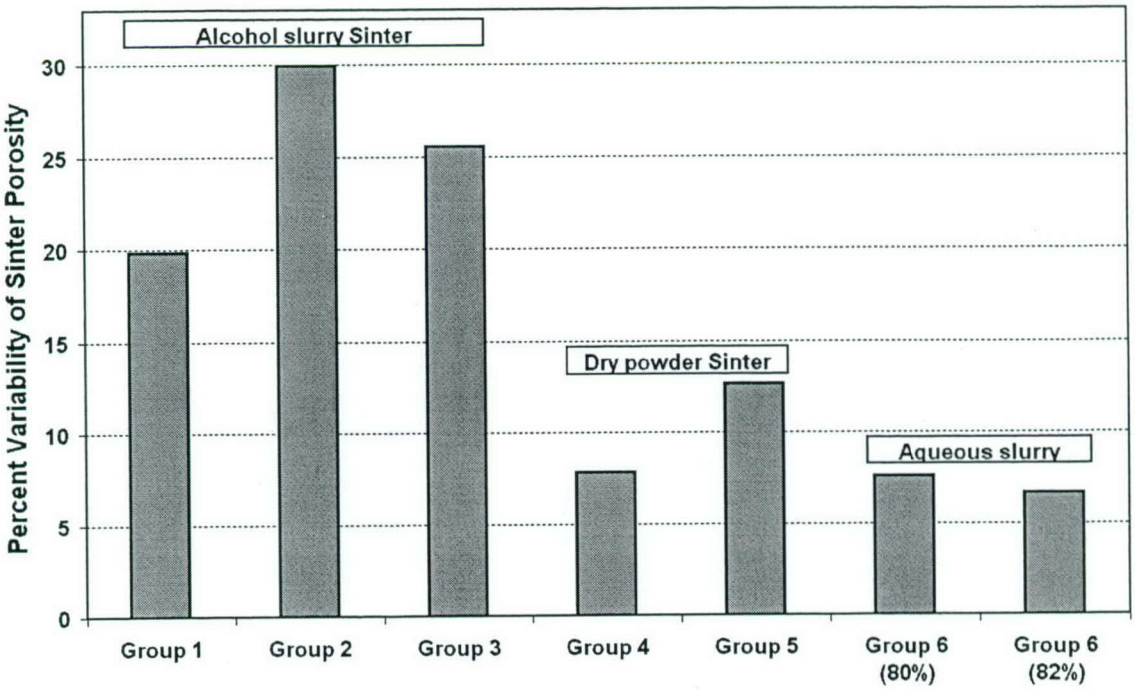

Figure 28. Variability in sinter porosity (as a percentage of overall average sinter porosity) for each type of sinter.

7. Conclusions

The porosity characteristics of nickel sinter made by three different processes has been evaluated by line-scan analysis of SEM images, and some significant differences in the internal structure of these different types of sinter have been observed. The structure of the alcohol-based slurry sinter tends to contain large internal voids as well as high-density aggregates of nickel that make the sinter porosity and pore sizes highly non-uniform. This type of nonuniformity was seen through the thickness of the alcohol-based slurry sinter, and was also found to be highly variable from one area of plaque to another.

The dry sinter and the water-based slurry sinter were both found to be much more uniform, in spite of having very different average internal pore sizes. The aqueous slurry sinter (and the uniform regions of the alcohol-based slurry sinter) displayed a smaller average pore size than did the dry-powder sinter. The aqueous slurry sinter process appears to offer a means to consistently obtain the smaller average pore sizes associated with the slurry process, along with the high degree of pore uniformity associated with the dry-powder process.

LABORATORY OPERATIONS

The Aerospace Corporation functions as an "architect-engineer" for national security programs, specializing in advanced military space systems. The Corporation's Laboratory Operations supports the effective and timely development and operation of national security systems through scientific research and the application of advanced technology. Vital to the success of the Corporation is the technical staff's wide-ranging expertise and its ability to stay abreast of new technological developments and program support issues associated with rapidly evolving space systems. Contributing capabilities are provided by these individual organizations:

Electronics and Photonics Laboratory: Microelectronics, VLSI reliability, failure analysis, solid-state device physics, compound semiconductors, radiation effects, infrared and CCD detector devices, data storage and display technologies; lasers and electro-optics, solid-state laser design, micro-optics, optical communications, and fiber-optic sensors; atomic frequency standards, applied laser spectroscopy, laser chemistry, atmospheric propagation and beam control, LIDAR/LADAR remote sensing; solar cell and array testing and evaluation, battery electrochemistry, battery testing and evaluation.

Space Materials Laboratory: Evaluation and characterizations of new materials and processing techniques: metals, alloys, ceramics, polymers, thin films, and composites; development of advanced deposition processes; nondestructive evaluation, component failure analysis and reliability; structural mechanics, fracture mechanics, and stress corrosion; analysis and evaluation of materials at cryogenic and elevated temperatures; launch vehicle fluid mechanics, heat transfer and flight dynamics; aerothermodynamics; chemical and electric propulsion; environmental chemistry; combustion processes; space environment effects on materials, hardening and vulnerability assessment; contamination, thermal and structural control; lubrication and surface phenomena. Microelectromechanical systems (MEMS) for space applications; laser micromachining; laser-surface physical and chemical interactions; micropropulsion; micro- and nanosatellite mission analysis; intelligent microinstruments for monitoring space and launch system environments.

Space Science Applications Laboratory: Magnetospheric, auroral and cosmic-ray physics, wave-particle interactions, magnetospheric plasma waves; atmospheric and ionospheric physics, density and composition of the upper atmosphere, remote sensing using atmospheric radiation; solar physics, infrared astronomy, infrared signature analysis; infrared surveillance, imaging and remote sensing; multispectral and hyperspectral sensor development; data analysis and algorithm development; applications of multispectral and hyperspectral imagery to defense, civil space, commercial, and environmental missions; effects of solar activity, magnetic storms and nuclear explosions on the Earth's atmosphere, ionosphere and magnetosphere; effects of electromagnetic and particulate radiations on space systems; space instrumentation, design, fabrication and test; environmental chemistry, trace detection; atmospheric chemical reactions, atmospheric optics, light scattering, state-specific chemical reactions, and radiative signatures of missile plumes.